Microstructural Coarsening Kinetics and Mechanical Property Changes in Long-Term Aged Sn-Pb-Sb Solder Joints

D.F. Susan, R.A. Wheeling[1], S.M. Williams, J. Yang, and C.E. Jaramillo

Metallurgy and Materials Joining Department, Sandia National Laboratories, Albuquerque, NM 87185 USA
dfsusan@sandia.gov

[1]Medtronic Inc., MECC, Brooklyn Center, MN 55430 USA

Abstract

Tin-lead-antimony (50Sn-47Pb-3Sb wt.%) soldered assemblies were mechanically tested approximately 30 years after initial production and found to have solder joints of reduced strength. The microstructure of this solder alloy exhibits a ternary eutectic structure with Sn-rich, Pb-rich, and SnSb phases. Accelerated aging was performed to evaluate solder microstructural coarsening and associated strength of laboratory solder joints to correlate these properties to the "naturally aged" solder joints. Isothermal aging was conducted at room temperature, 55, 70, 100, and 135°C and aging times that ranged from 0.1 to 365 days. The coarsening kinetics of the Pb-rich phase were determined through optical microscopy and image analysis methods established in previous studies on binary Sn-Pb solder. A kinetic equation was developed with time exponent n of 0.43 and activation energy of 24000 J/mol, suggesting grain boundary diffusion or other fast diffusion pathways controlling the microstructural evolution. Compression testing and Vickers microhardness showed significant strength loss within the first 20-30 days after soldering; then, the microstructure and mechanical properties changed more slowly over long periods of time. By combining accelerated aging data and the microstructure-based kinetics, strength predictions were made that match well with the properties of the actual soldered assemblies naturally aged for 30 years. However, aging at the highest temperature of 135°C produced anomalous behavior suggesting that extraneous aging mechanisms are active. Therefore, data obtained at this temperature or higher should not be used. Overall, the combined microstructural and mechanical property methods used in this study confirmed that the observed reduction in strength of ~30-year-old solder joints can be accounted for by the microstructural coarsening that takes place during long-term solid-state aging.

Sandia National Laboratories is a multimission laboratory managed and operated by National Technology and Engineering Solutions of Sandia, LLC., a wholly owned subsidiary of Honeywell International, Inc., for the U.S. Department of Energy's National Nuclear Security Administration under contract DE-NA0003525.

Keywords Solder, microstructure, kinetics, microhardness, compression, strength

Introduction

It is well-known that solder joints experience microstructural aging under isothermal or thermal cycle conditions that can affect the mechanical properties of the joints [1-8]. The reason is that, for many solder alloys, room temperature represents a relatively high homologous temperature, T_h, defined as the ratio of service temperature to solidus temperature, $T_h = T_{service}/T_{solidus}$, both temperatures expressed in K. For example, at room temperature (298K), eutectic Sn-Pb solder ($T_{solidus}$=456K) would be at a T_h equal to 0.65. The ternary tin-lead-antimony (Sn-Pb-Sb) solders have comparable melting temperature ranges to that of the eutectic Sn-Pb alloy. The Sb addition gives the ternary solders increased strength and creep resistance through solid-solution strengthening of the β-Sn phase as well as the formation of SnSb particles within the microstructure [9,10]. Previous work by Lampe on the alloy of interest here, 50Sn-47Pb-3Sb wt.%, (62.6Sn-33.7Pb-3.7Sb, at.%), showed a brief initial increase in hardness followed by significant softening during the first 100 hours after solidification and then a gradual decrease in hardness after that [9]. The study by Lampe reported on aging effects only up to 60 days after solidification and did not include extensive microstructural characterization. Other studies on ternary Sn-Pb-Sb solders were found in the literature, including creep investigations [11-17]. However, those studies did not examine very long-term solid-state aging or alloy compositions relevant to the current investigation.

A methodology to analyze isothermal aging of solders was developed by Vianco et al. using binary eutectic Sn-Pb solder [18-20]. The work established empirical relationships with Arrhenius temperature dependence for both interfacial intermetallic compound (IMC) growth

kinetics and Pb-rich phase coarsening within the Sn-Pb solder microstructure. A similar approach was taken in the present work to analyze the Pb-rich phase coarsening kinetics during isothermal aging of ternary Sn-Pb-Sb solder. The kinetics were analyzed according to the following expression:

$$x = x_0 + At^n \exp\left(-\Delta H/RT\right) \qquad (1)$$

where x is the mean Pb-rich particle size (area) in mm^2, x_0 is the as-fabricated baseline particle size, A is the pre-exponential constant, n is the time exponent, ΔH is the apparent activation energy (J/mol), R is the universal gas constant (8.314 J/mol-K), and T is temperature (K). This kinetics expression was used in previous studies [18-20]. Taking the logarithm of equation (1) gives equation (2) below:

$$\ln(x - x_0) = \ln A + n\ln(t) - \Delta H/RT \qquad (2)$$

Experimental accelerated aging data were fit to equation (2) using multivariable linear regression analysis. The independent variables were $\ln(t)$ and $1/T$; the dependent variable was $\ln(x - x_0)$. The output data were the intercept, $\ln(A)$, and the slopes of the two independent variables: the time exponent, n, and the parameter $\Delta H/R$. The latter slope value was multiplied by R to give the apparent activation energy, ΔH.

In one of the studies, Vianco et al. investigated the effects of cooling rate during solidification on the subsequent Pb-rich phase coarsening kinetics of Sn-Pb [19]. They found that fast diffusion mechanisms with low activation energy barriers characterized the samples that had undergone slower cooling rates. The mechanism likely originated from in-situ development of a recovery/recrystallization microstructure within the Sn-rich phase matrix of

the solder [21]. These conditions are considered relevant for the current work in which relatively large (bulk) solder specimens were employed -- with slower cooling rates than those encountered in small microelectronics solder joints.

The current investigation was motivated by mechanical testing of 50Sn-47Pb-3Sb solder joints that had been fielded for ~30 years. The mechanical properties of the aged solder assemblies were compared to data collected at the time of original manufacturing of the fielded solder joints. The geometry of the fielded solder joints of interest is shown in Fig. 1. Cylindrical nickel parts were soldered together as shown using Sn-Pb-Sb solder. To ensure proper wetting of the nickel parts, generous amounts of liquid flux were applied to all surfaces prior to solder reflow. The assemblies comprise a large structural solder joint, as opposed to small microelectronic solder joints often found in other studies. The large solder joints simulated bulk samples and, therefore, bulk cast Sn-Pb-Sb specimens were chosen for the accelerated aging study to correlate to the naturally aged assemblies in Fig. 1.

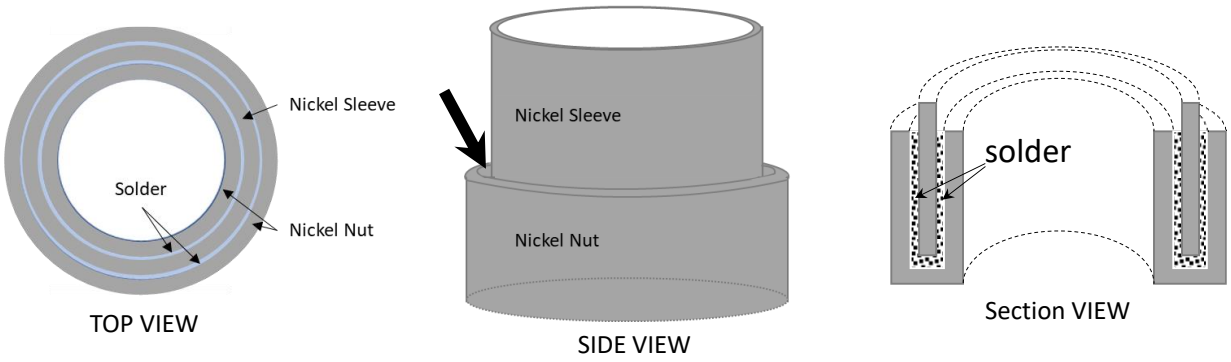

Fig. 1 Schematic diagram of structural solder joints made approximately 30 years ago with 50Sn-47Pb-3Sb solder.

The strength of the 30-year-old soldered assemblies was determined by pull testing the central Ni sleeve from the lower Ni nut; the maximum tensile load was recorded for each test. Figure 2 displays the data collected during original component manufacturing (open black circles) together with the test results obtained from assemblies after 30 years in the field (closed red squares). A total of 382 assemblies from several lots were tested at the time of manufacture; 27 assemblies were tested following 30 years in the field. The latter assemblies had their lot numbers correlated to the lots from the original 382 assemblies. Figure 2 shows that the soldered assemblies, which were tested after ~30 years in the field, exhibited lower average strength than the manufactured assemblies.

The original assembly designers understood that solder properties can change over time, especially in the near-term, so “stabilization treatments” were applied to the post-soldered assemblies prior to mechanical testing. The stabilization treatments employed were either 20 days at room temperature (25°C) or 3 days at 100°C. It is not known how the two

different stabilization treatments were partitioned among the original manufactured parts shown in Fig. 2. Nevertheless, the mechanical test results in Fig. 2 offer a rare opportunity to compare the mechanical properties of long-term, solid-state aged solder joints to those of as-manufactured (plus-stabilized) solder joints.

The present investigation had two objectives. The first objective was to systematically determine if solid-state metallurgical aging of the solder can account for the observed decrease in strength of the 50Sn-47Pb-3Sb soldered assemblies. The second objective was to explore the assertion that accelerated aging experiments at elevated temperatures are a viable means of predicting the long-term microstructures and mechanical performance of solder joints aged at ambient temperature.

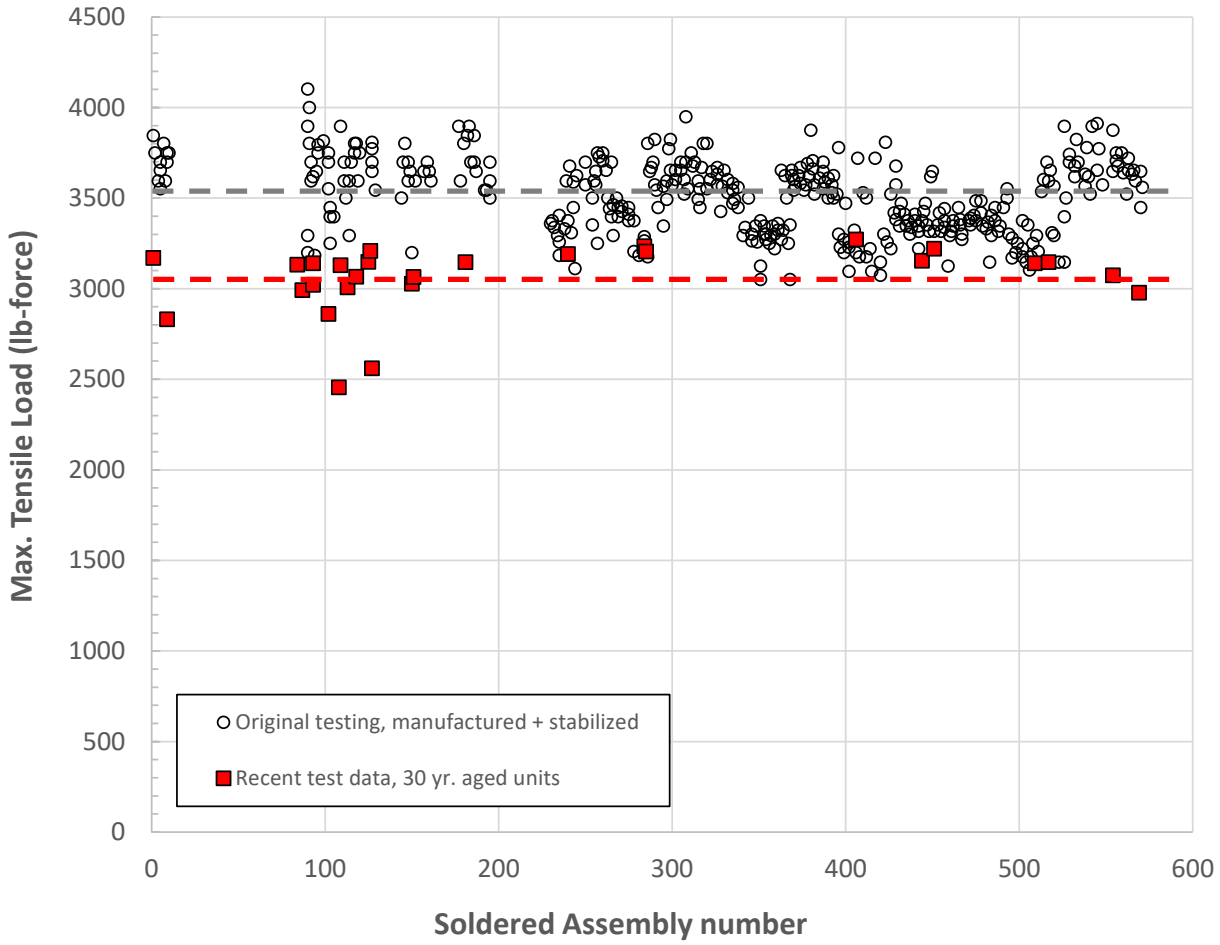

Fig. 2 Mechanical test data from original Sn-Pb-Sb solder joints as-manufactured plus 20 days at room temperature or 3 days at 100°C. Compared to strength data from 30-year-old soldered assemblies from the same manufacturing lots.

Microstructural coarsening of the Sn-Pb-Sb bulk solder was the main aging parameter and strength of the bulk solder was the primary response variable. However, the interface microstructures can also affect solder joint strength. Although the majority of the pull-tested

solder joints failed within the bulk solder, the joints did show a small amount of interfacial or near-interface failure, which required further consideration.

The interfacial failure mode is influenced by the intermetallic compound (IMC) that forms during soldering and grows during solid-state aging between the nickel substrates and the Sn-Pb-Sb solder. The IMC is likely a $Ni_3(Sn,Sb)_4$ phase. Different contributions by the interfacial failure mode could account for the variability in the original as-manufactured test data (Fig. 2). The standard deviation was 6% of the mean value, i.e. 3508 +/- 201 lbs. force. The overall range of strength values spanned almost 30% about the mean. The strength of the aged joints was 13% lower on average; but, the standard deviation was about the same at ~6%, being 3058 +/- 191 lbs. force. The strength range of the aged solder joints was 27%, only slightly less than that of the unaged samples. Therefore, the data *scatter* was not a function of the bulk solder microstructure and the associated aging. The role of the interface failure mode would require empirical validation, which was beyond the scope of this study. An accounting of other manufacturing parameters, which could have been responsible for the strength variability, included slightly different joint (gap) geometries; different amounts of solder within the joints; the amount of porosity within the joints; and microstructural variability caused by variations of soldering temperatures and cooling rates between samples.

Experimental Procedure

The 50Sn-47Pb-3Sb (wt.%) solder was obtained from a commercial supplier. The test samples were melted and cast into cylindrical molds of 10 mm diameter by 20 mm length. An

initial specimen microstructure was characterized as soon as possible after casting. Additional samples were aged at room temperature for up to 365 days. Other test specimens were exposed to accelerated aging at 55, 70, 100, and 135°C in air and for similar time periods up to 365 days. The temperatures were chosen based on the body of work developed by Vianco et al. on binary Sn-Pb [18-20].

At prescribed aging time intervals, specimens were prepared metallographically and the solder microstructures were examined. To quantify the volume fraction and average particle size (represented by particle area in mm^2) of the Pb-rich phase, quantitative image analysis (QIA) was performed using Image-J software (U.S. National Institutes of Health, Bethesda MD). The QIA was performed on multiple micrographs obtained at 500 times magnification. Lower magnifications caused small Pb-rich particles to be omitted from the analysis. Several thousand particles were analyzed at each aging condition to minimize the standard deviation in particle diameter, similar to the approach by Vianco et al. [18]. As such, the scatter reported for the Pb-rich phase size is due to actual microstructural variability and was not a sampling effect. Microstructural analysis was also performed on the 30-year aged soldered assemblies (from Fig. 2) and compared to the experimentally accelerated aged specimens. A total of four assemblies and six 500X micrographs were analyzed from the 30-year-old assemblies.

Scanning electron microscopy (SEM) and energy dispersive spectroscopy (EDS) were performed to further characterize the microstructure. Because of the overlap of EDS peaks between Sn and Sb, electron probe microanalysis (EPMA) with wavelength dispersive spectroscopy (WDS) was performed to determine, qualitatively, the distribution of SnSb phase in the microstructure by distinguishing it from the matrix β-Sn phase. The accelerating voltage

was 15kV and beam current was 20 nA. SnSb and β-Sn show the same contrast in optical microscopy when viewed in the as-polished condition, and therefore, it was not possible to perform QIA to separately quantify the SnSb phase.

Specimens representing each combination of aging time and temperature, were tested with Vickers microhardness indentation performed with a Struers Durascan-70 tester (Struers Ltd., Denmark). The test parameters were a 50 gram load and 15 second dwell time. The average and standard deviation of 16 hardness tests were reported for each specimen.

Compressive stress-strain tests were also performed on an MTS load frame (MTS Systems Corp., Eden Prairie, MN). All tests, which were performed on both as-cast and aged test samples, were done at room temperature. The specimens were compressed by 2.4 mm at a constant displacement rate of 1mm/min, resulting in a constant strain rate of 8.3×10^{-4} sec^{-1}. The 0.2% offset yield strengths were determined and the average and standard deviation reported for seven tests representing each of the specimen aging conditions. Compressive testing was chosen for simplicity of the test regimen and fixturing. The strength results will be compared to the hardness and *shear* strength data collected by Lampe on the same solder alloy; Lampe's specimens were aged for up to 60 days at room temperature [9].

Results and Discussion

50Sn-47Pb-3Sb (wt.%) Solder Microstructure

The 50Sn-47Pb-3Sb (wt.%) solder microstructure is shown in Fig. 3 for an as-cast cylindrical specimen from the current study and a 30-year aged solder joint at the same magnification. Clearly, coarsening of the dark Pb-rich phase has taken place in the long-term aged solder. The larger Pb-rich phase particles grew at the expense of smaller particles. Microstructural coarsening, which involves both Pb-rich phase coarsening as well as grain growth in the Sn-rich matrix phase (not obvious in Fig. 3), contribute to reduction in mechanical strength over time. In the as-cast condition in Fig. 3, some larger proeutectic Pb-rich dendrites are found, which is an important consideration for measurement of overall (average) Pb-rich phase size and distinguishes the microstructure of this alloy from that of the eutectic SnPb solder. During aging/coarsening, the proeutectic Pb-rich dendrites become less distinct within the microstructure. Small regions of Sn-rich phase (bright contrast) are also found within the Pb-rich particles. Precipitation of Sn-rich phase occurs within the Pb-rich phase due to a supersaturation of Sn; the precipitation begins during solidification and cooling, and will continue during long-term aging. It is apparent in Fig. 3 that the Sn-rich precipitates also coarsen along with their surrounding Pb-rich phase regions.

The microstructures displayed in Fig. 3 appear similar to binary SnPb solder microstructures. Already mentioned were the pro-eutectic Pb-rich phase dendrites present in the Sn-Pb-Sb alloy. Another difference is the appearance of the SnSb phase. Figure 4a shows an optical micrograph taken at high magnification with a closed main aperture to highlight

topographical differences due to polishing. The SnSb phase is discernible by the surface relief because it has higher hardness than the Sn-rich and Pb-rich phases. Figure 4a highlights the fact that Sn-Pb-Sb solder solidifies as a ternary eutectic microstructure as opposed to the binary SnPb case.

Further investigation was made of the SnSb phase using scanning electron microscopy. Fig. 4b shows a high-magnification, backscattered electron (BSE) image of the microstructure. It is also difficult to discern the SnSb phase from the Sn-rich matrix with BSE/SEM because the two phases have similar atomic numbers so the contrast is very weak. Note, the BSE contrast is flipped compared to optical microscopy – the Pb-rich phase is bright and the Sn-rich matrix is dark. Based on calculations of backscatter coefficient for pure Sn and pure Sb (atomic numbers 50 and 51), the difference in contrast is only 0.8% [22]. The BSE contrast between the SnSb phase (~50/50 SnSb) and the Sn-rich phase (with some Pb solubility) is even less. Chemical etching is necessary to reveal the SnSb phase; see Fig. 4c. The SnSb phase is not attacked by the etchant and appears somewhat brighter than the Sn-rich phase matrix, but the etchant clearly delineates the boundary surrounding the SnSb phase.

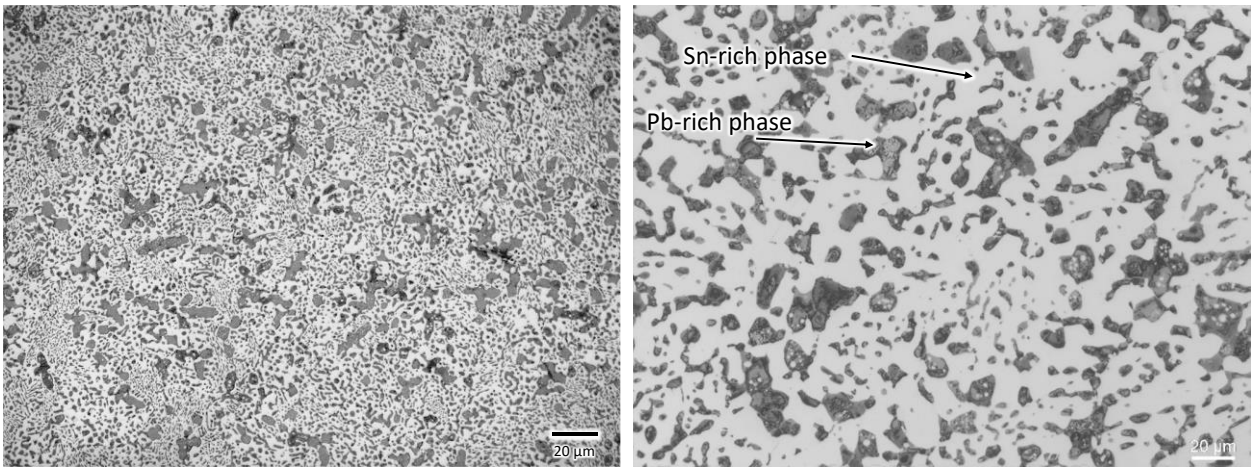

Fig. 3 Microstructures of as-solidified Sn-Pb-Sb solder (left) from the current study compared to 30-year aged solder from a field-return component at the same magnification (right). Scale bars = 20 microns. (light optical microscopy, as-polished)

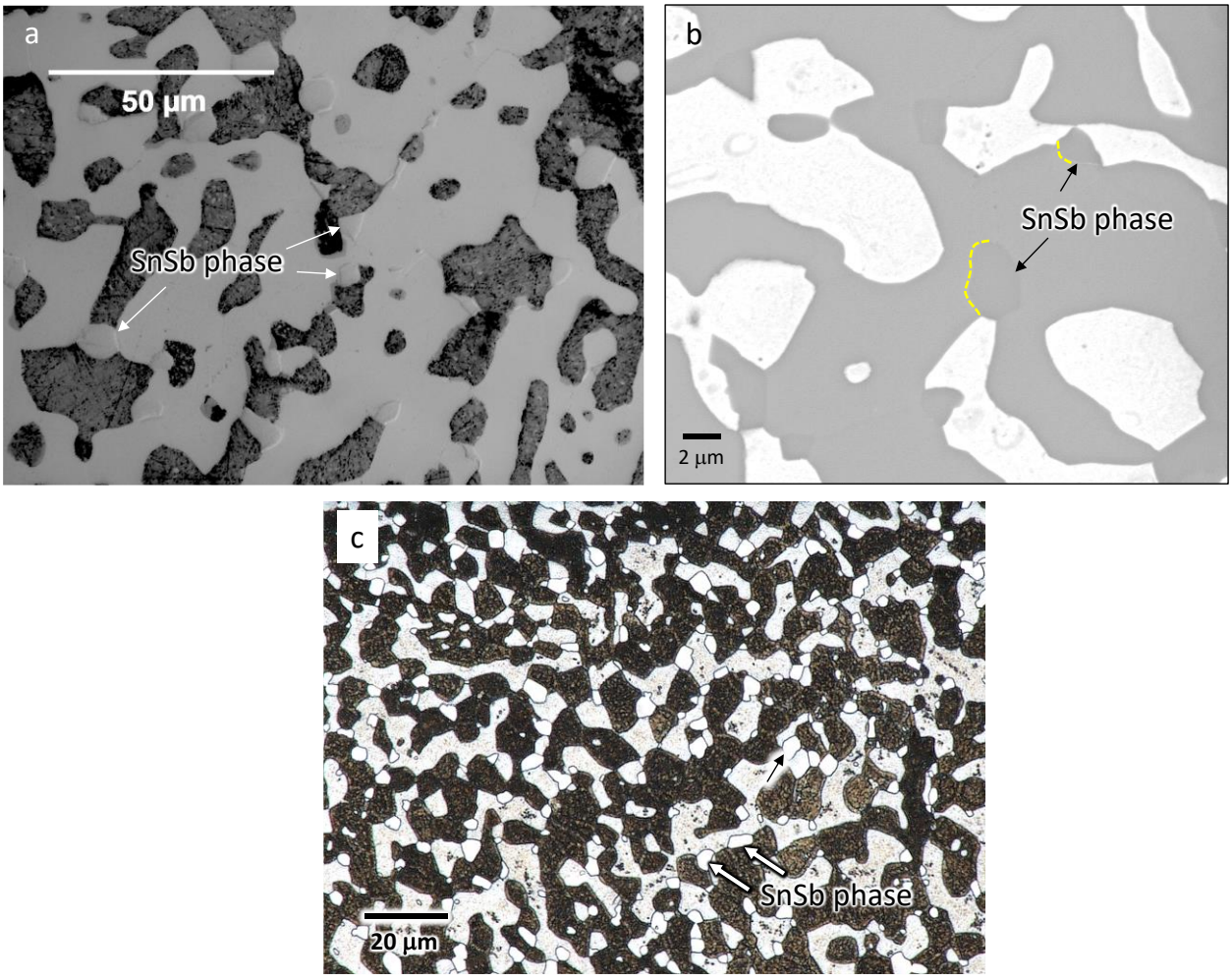

Fig. 4 a) Optical microscopy with closed aperture to highlight polishing relief of the SnSb phase. b) Backscatter electron micrograph of Sn-Pb-Sb solder (accelerating voltage 20kV). SnSb particles are delineated with dashed lines. c) Optical microscopy of etched microstructure, Etchant: 2mL HCl, 2g $FeCl_3$, 30mL H_2O, 60mL ethanol

The EDS and EPMA/WDS techniques were employed to further characterize the Sn-Pb-Sb microstructure and, in particular, the SnSb particle phase. Figure 5 displays EDS elemental maps and spectrum imaging obtained using the AXSIA method [23]. The EDS elemental maps

show the effects of the significant overlap of Sn and Sb peaks. Although some increased intensity is shown for Sb in the SnSb regions, the maps for Sn and Sb, because the intensities are auto-scaled, are misleading in terms of the actual distribution of Sb in the microstructure. The spectrum imaging technique is able to separate the three phases well by combining multiple peaks in the EDS spectrum (as opposed to a single EDS elemental map). Figure 6 shows the EPMA/WDS results for comparison. The WDS system readily distinguishes between Sn and Sb because the peaks don't overlap in WDS – hence, a better capability to resolve the two elements. First, the maps show the expected composition of SnSb of 50Sn/50Sb and that the SnSb phase is distributed uniformly throughout the microstructure. Second, the Sb map also indicates that the solubility limit of Sb in the Sn-rich phase is 5-10% (blue background in the Sb map), which is consistent with the Sn-Pb-Sb ternary phase diagram [24]. In contrast, there is very little solubility for Sb in the Pb-rich phase (black background in the Sb map), which is also consistent with the ternary Sn-Pb-Sb isothermal section. Third, image analysis of the Sb map indicates that the SnSb phase comprises about 4 vol. % of the 50Sn-47Pb-3Sb microstructure.

However, higher-fidelity quantitative image analysis of the SnSb phase was not carried further in this work due to resolution limitations of optical microscopy. Therefore, in the image analysis results described below, the SnSb phase is included as part of the Sn-rich matrix phase. Nevertheless, the presence of the SnSb phase can affect the long-term aging kinetics of the solder. High-angle and/or incoherent boundaries likely exist between the SnSb particles and both the Sn-rich and Pb-rich phases. Incoherent grain boundaries have been associated with fast diffusion paths of low activation energies in previous studies, thereby altering the thermodynamics and rate kinetics of the coarsening process(es) [25-27].

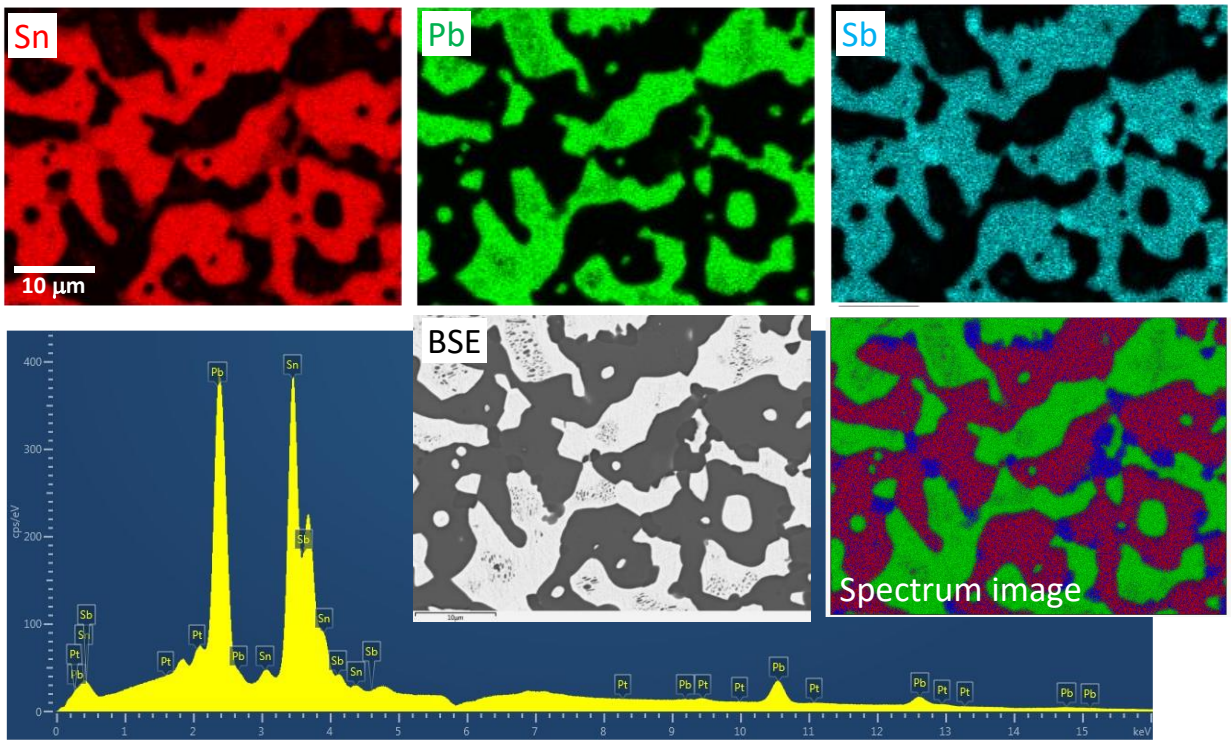

Fig. 5 Elemental EDS maps, EDS spectrum, and spectrum imaging of Sn-Pb-Sb solder. Specimen was cast and then aged for 200 days at room temperature. Accelerating voltage: 20 kV

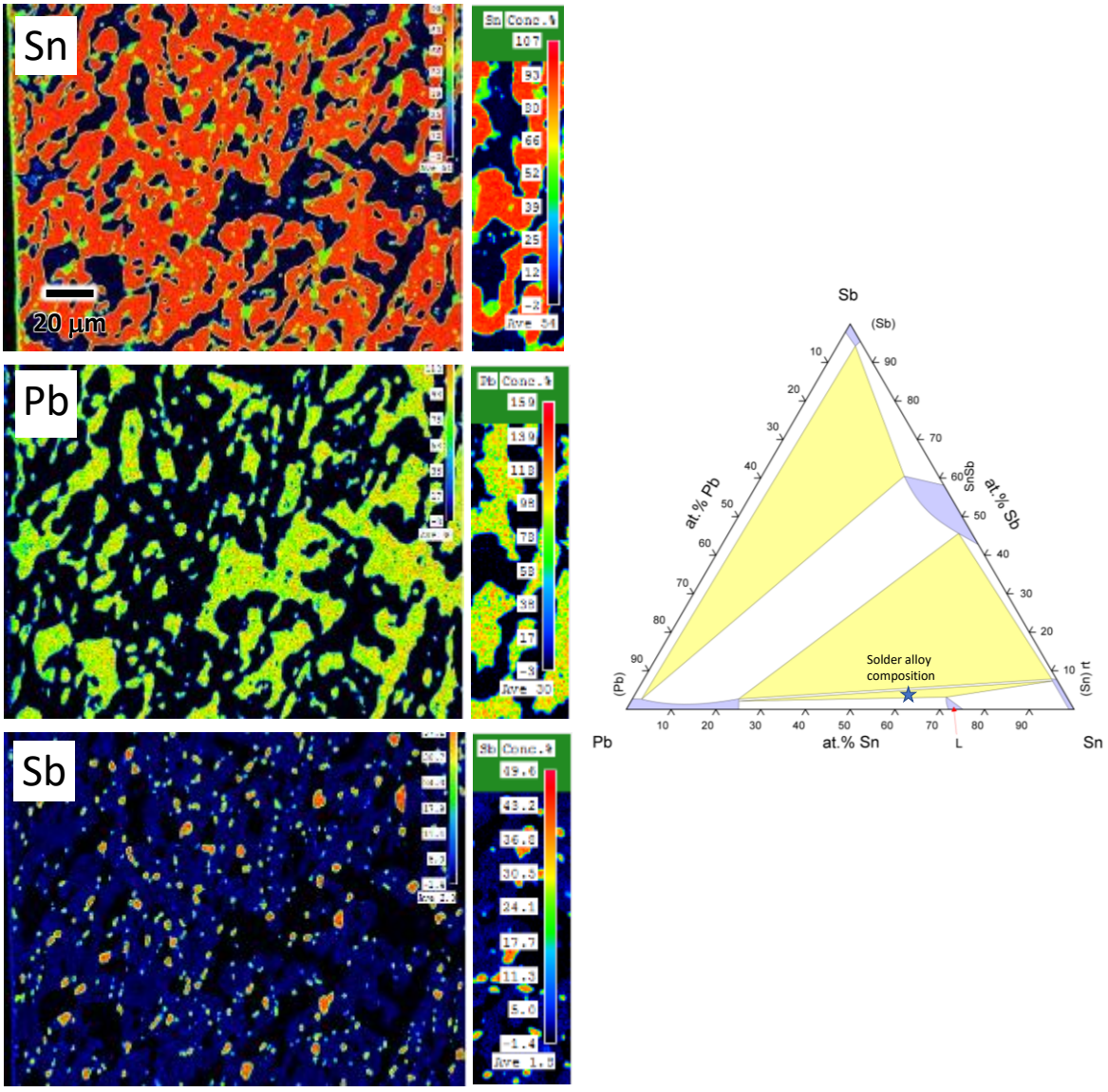

Fig. 6 Quantitative EPMA/WDS maps of Sn, Pb, and Sb. Specimen of 30 yr. aged solder joint. 15 kV, 20 nA beam current. Along with Sn-Pb-Sb phase diagram isothermal section at 189°C [24].

Kinetics of Pb-rich Phase Coarsening in 50Sn-47Pb-3Sb Solder

For the accelerated aged specimens, an overview of microstructural development across time and temperature is shown in Fig. 7 with individual examples of the Sn-Pb-Sb solder

microstructure at the same magnification for each aging interval. The as-cast microstructure and the 20-day RT and 55°C specimens have fine-scale microstructures with evidence of partially lamellar eutectic colonies. Coarsening of the Pb-rich phase is apparent for increasing time and temperature as expected for a diffusion driven process. In addition, the eventual polygonization of the Pb-rich phase is also observed, especially at the highest temperature and longest time, i.e. 135°C for 365 days. The development of straight faceted grain boundaries in the Sn-rich phase and interphase Sn-rich/Pb-rich boundaries represents a largely stabilized microstructure; little further coarsening would be expected of the solder. As a qualitative comparison, a micrograph from a 30-year naturally aged solder joint is superimposed over the array of accelerated aged specimens. The 30-year microstructure corresponds generally to accelerated aging conditions of 70C-100°C for 100-200 days, although some similarity was found between it and the microstructures represented by other accelerated age conditions. The qualitative correspondence of the 30-year aged solder microstructure and the laboratory accelerated aged microstructures suggests that the approach used here and in previous studies, for which long-term naturally aged specimens are typically not available, is reasonable for approximating the long-term naturally aged condition. A fully quantitative analysis is developed in the following discussion using image analysis results and the rate kinetics equations.

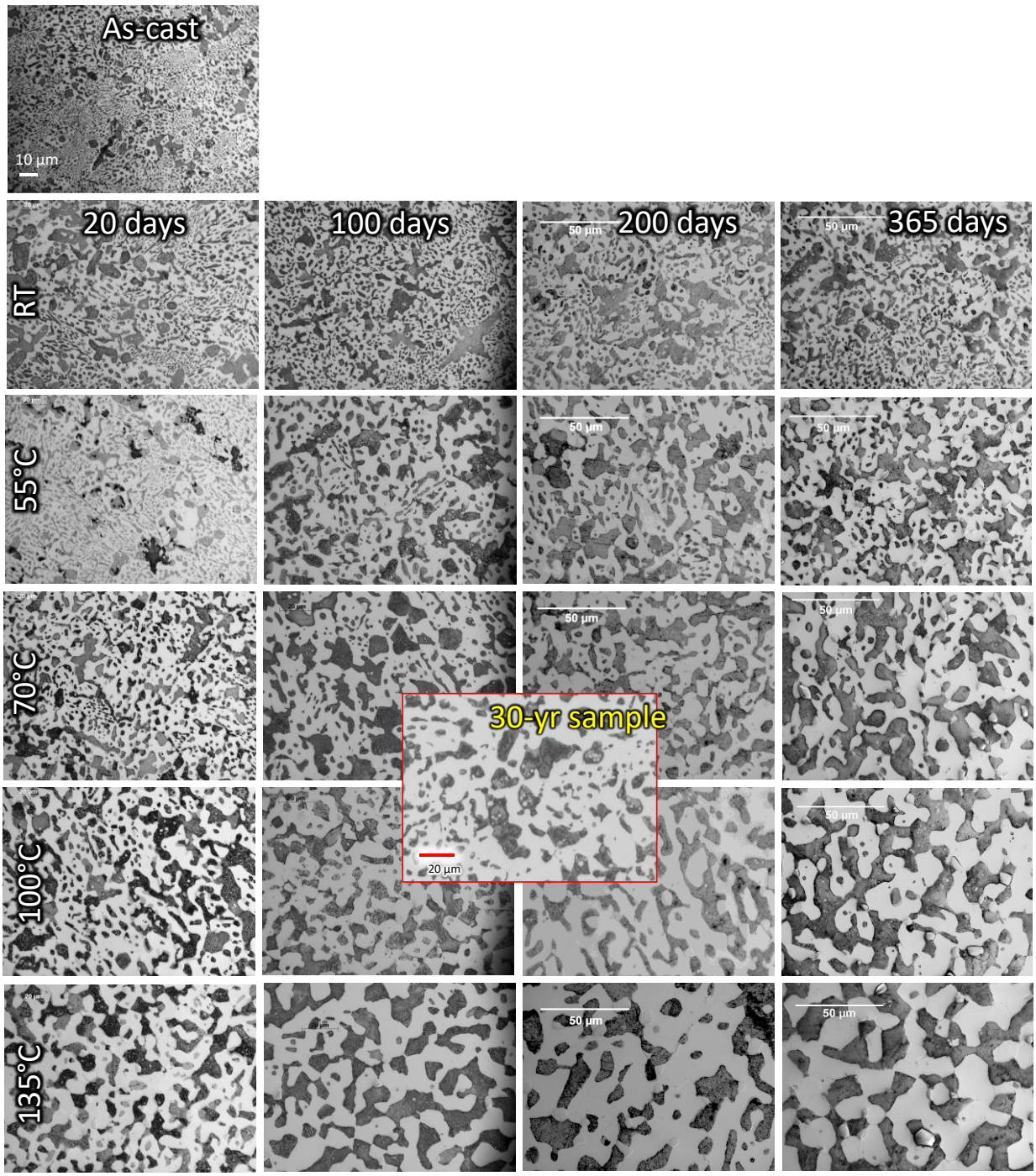

Fig. 7 Optical microscopy of room temp. and accelerated aged Sn-Pb-Sb up to 365 days. Each row displays an aging temperature and each column gives an aging time. A 30-year (naturally aged) solder joint microstructure is superimposed for comparison.

The first step in the kinetics analysis was to determine the baseline value of Pb-rich phase size, x_0. This was obtained through image analysis of the as-cast 50Sn-47Pb-3Sb samples as soon as possible after solidification and metallographic sample preparation. Upon analysis of over 3000 particles at 500 times magnification, the baseline Pb-rich particle size was determined to be:

$$x_0 = 3.75 \times 10^{-6} \text{ mm}^2$$

This value is similar but slightly larger than the 3.2 x 10^{-6} mm^2 value found in previous work on binary SnPb solder with "microelectronic" solder joints [18-20]. The larger initial particle size here might be attributed to the larger bulk solder specimens and subsequent slower cooling rate in the current study. Or, the larger particle size was simply due to differences in microstructural development of the two solder compositions. Note that significantly smaller x_0 values in the range 0.5 to 2.54 x 10^{-6} mm^2 were determined in the SnPb cooling-rate investigation by Vianco et al. (cooling rates from 0.1 to 100 °C/min) [19].

Analysis of the rate kinetics data for the accelerated aged samples revealed a slight temperature dependence at the lower (RT, 55°C) and higher (135°C) temperatures. Therefore, the intermediate aging temperatures of 70°C and 100°C were used to develop the rate equation. The selection of this temperature regime is consistent with prior accelerated aging studies [18,19]. A summary of the Pb-rich particle size data for these two temperatures is shown in Fig. 8. Based on multilinear regression analysis, the kinetics equation for the Pb-rich phase coarsening in Sn-Pb-Sb solder is given below:

$$x = 3.75 \times 10^{-6} + 8.5 \times 10^{-5} \, t^{0.43} \exp(-24200/RT) \qquad (3)$$

The units in eq. 3 were as follows: x in mm^2 (3.75 X 10^{-6} mm^2); t in (s); 24200 J/mol; 8.5 x 10^{-5} $mm^2/s^{0.43}$; T (K); and the parameter, R, is the universal gas constant 8.314 J/mol-K.

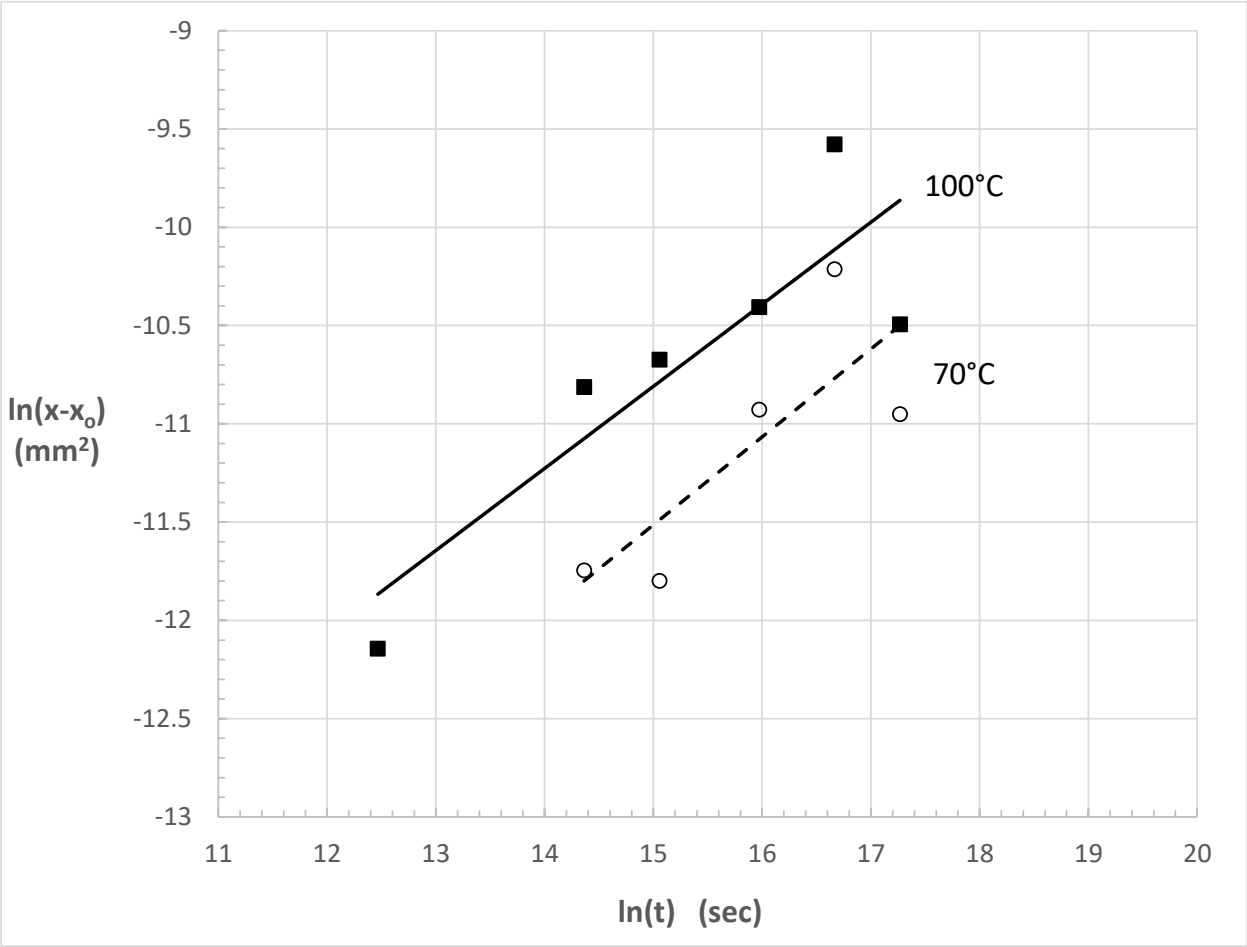

Fig. 8 Plot of mean Pb-rich phase particle size from 50Sn-47Pb-3Sb aged at 70°C and 100°C for up to 365 days.

The equation developed here has a higher time exponent, 0.43 with standard deviation of ± 0.09, compared to previous studies on SnPb solder with n-values between 0.23 and 0.36 [18-20]. This suggests the coarsening process in the present experiments tends more toward a

bulk diffusion controlled process as indicated by a value of n = 0.5 rather than a process controlled by fast diffusion paths. Vianco et al. suggested that differences in the amounts of *in situ* recovery and/or recrystallization could take place for solder solidified under different cooling rates resulting in slight variations to the diffusion mechanism. The bulk samples used here could exhibit lower grain boundary area and, therefore, fewer fast-diffusion paths due to slower cooling rates. This hypothesis is also supported by the larger initial Pb-rich phase size, x_0, when compared to those previous investigations. However, the presence of the SnSb particle phase in Sn-Pb-Sb alloy offers an additional set of interphase boundaries not found in SnPb solder, which could assist the diffusion process.

The low apparent activation energy ΔH of -24,200 J/mol (± 8835), however, does indicate the presence of a fast diffusion process. The value of -24,200 J/mol is within the range of values reported previously for binary SnPb solder coarsening [18-20]. The activation energy appears to be lower than those typical of grain boundary or interphase boundary diffusion, which are typically 40-60% of the values for bulk diffusion [28-31]. For context, the activation energies for Sn and Pb self-diffusion were 94 and 101 kJ/mol determined by Decker or 99 and 100 kJ/mol as determined by Mehrer and Seegar [29,30].

Low activation energies such as those observed in the present investigation and in previous studies suggest the occurrence of diffusion mechanisms that arise when the solubilities of the solute elements are very low in the solvent metal [20,32]. For example, Yeh and Huntington showed that diffusion of Ni in Sn was accompanied by very low activation energies in the 15-25 kJ/mol range [32]. A similar process could be governing Pb (and possibly Sb) diffusion in the Sn-rich phase because Pb has very low solubility in Sn.

An alternative scenario is that the low activation energy was the result of microstructural variations resulting from the initial cooling step or changes to the microstructure during subsequent aging in parallel with Pb-rich phase coarsening. For example, the recovery process removes point defects which can act as sinks for Pb atoms within the Sn matrix that may impede the diffusion kinetics. Moreover, recrystallization within the Sn matrix can provide increased grain boundary pathways for fast diffusion, although this idea contradicts the argument made above with regard to the higher n-value of 0.43. In any case, the proposed microstructural changes are more likely to prevail during slower cooling from initial solidification and/or be enhanced during higher accelerated aging temperatures. Overall, the time exponent, n, and the activation energy ΔH correspond best to those observed for SnPb solder by Vianco et al. for initial cooling rates of 100°C/min and 10°C/min, respectively. This observation suggests that the possible cooling rate experienced by the Sn-Pb-Sb samples was between these two values. Given the likelihood of a cooling rate effect, future studies should control the cooling rate of test specimens prior to subsequent solid-state aging.

An objective of the present investigation was to correlate the Sn-Pb-Sb microstructure following accelerated aging to the microstructure observed after natural aging for ~ 30 years. This analysis determines the amount of accelerated aging time (s) required at an accelerated aging temperature, T, to predict the same degree of aging – i.e., the same Pb-rich phase size – at room temperature (years). Equation (2) was solved for time t, in seconds, giving Equation (4):

$$t = \{[(x - x_0)/A]/[\exp(-\Delta H/RT)]\}^{1/n} \qquad (4)$$

The predicted time values were converted to years. In Eq. (4), the values used for x, Pb-rich phase size, were obtained from Eq. (3) above for each combination of accelerated aging temperature and time. For each given Pb-rich phase size, x, Eq. (4) was then solved using room temperature (298K) for T. In this manner, the predicted "natural aging" time was found for which a corresponding Pb-rich phase size (from accelerated aging) would be encountered. Those aging times are shown in Fig. 9 (y-axis), again in units of years of aging at room temperature. The actual experimental aging time for the five temperatures employed in the experimental work on 50Sn-47Pb-3Sb solder are shown on the x-axis. Although the kinetic equation was developed using only data from 70°C and 100°C, Fig. 9 displays the predicted room temperature aging conditions for accelerated aging performed at all temperatures in this study, from room temp. to 135°C.

Figure 9 gives a graphical representation of the acceleration factors for each accelerated aging temperature. The numerical acceleration factors can easily be obtained by a ratio of aging time at elevated temperature, the solution of Eq.(4) for example at 55°C (328K), to the aging time at room temperature, Eq. (4) solved at room temp. (298K). The terms A and $(x - x_0)$ cancel out and Eq. (5) is obtained:

$$\text{Acceleration time factor (for } T_{acc}) = \frac{[\exp(-\Delta H/RT_{acc})]^{1/n}}{[\exp(-\Delta H/R(298)]^{1/n}} \qquad (5)$$

In Eq. (5), T_{acc} represents any accelerated aging temperature and 298K is used for room temperature. Using Eq. (5), acceleration factors of 8.0, 19.8, 97.3, and 462.9 are obtained for aging temperatures of 55, 70, 100, and 135°C. These factors represent the constant offsets

between the accelerated aging curves in Fig. 9 and the room temperature aging curve (black line and symbols).

The 30-year simulated natural aging condition is also highlighted by the dashed line in Fig. 9. The plot indicates that the most practical accelerated aging condition that would simulate 30 years of natural aging would be roughly 100 days at 100°C. This condition matches well with the qualitative microstructural comparison shown in Fig. 7 for 30-year aged solder joints. Other accelerated aging conditions from the present study giving similar predictions of room temperature aging would be 20 days at 135°C or 365 days at 70°C (predicting 25 or 20 years of natural aging, respectively). For a more quantitative comparison with the 30-year natural aged condition, image analysis was performed on six micrographs from actual 30-year aged solder joints (examples in Figs. 3 and 7). The average Pb-rich phase size was 3.91 X 10^{-5} mm^2 (± 12%). Using Equation (4), this corresponds to a predicted age of 52 ± 17 years. This is deemed a reasonable estimate given the uncertainties about the original soldering process 30 years ago, the unknown original value of x_0 for the 30-year aged joints, and the exact storage conditions of the aged assemblies. Alternatively, the kinetic equation can be solved to predict what storage temperature would be required to produce the observed Pb-rich phase size in 30 years. In this case, the predicted storage temperature was 33°C (91.4°F). This temperature is slightly higher than room temperature and may also include elevated temperature storage, qualification testing, and acceptance testing regimens performed over the solder joints' lifecycle.

Given the higher predicted age of 52 +/- 17 years, another factor to consider is that other mechanisms contributed to Pb-rich phase coarsening besides isothermal aging.

Thermomechanical fatigue (thermal cycling) can accelerate microstructural coarsening, especially in localized regions [5,20,33-39]. Thus, it is important to emphasize that the Pb-rich phase coarsening kinetics of the present study apply only to *isothermal* aging. In engineering practice, to properly predict performance of a soldered assembly, isothermal accelerated aging is a suitable starting point to produce Pb-rich phase coarsening and a lower strength solder condition. However, the isothermal aging should be accompanied by any thermal mechanical fatigue conditions expected in the lifecycle of the solder joint.

The isothermal aging data can also be used to pinpoint actual solder joints that display a greater degree of Pb-rich phase coarsening than predicted by isothermal aging kinetics. Such an observation would suggest that other coarsening mechanisms are operative (thermomechanical fatigue, mechanical stress, etc.) in the soldered assembly. In that case, the current isothermal accelerated aging approach would be used to highlight contributions by the other mechanisms at play.

Finally, caution should be used when attempting to correlate natural aging times with accelerated aging at temperatures equal to or greater than 135°C despite the convenience of shorter test times. Higher aging temperatures can introduce additional metallurgical mechanisms to the Pb-rich phase coarsening process, that is, mechanisms that would not be operative during long-term aging at room temperature. More discussion is provided later below with respect to the 135°C limiting case.

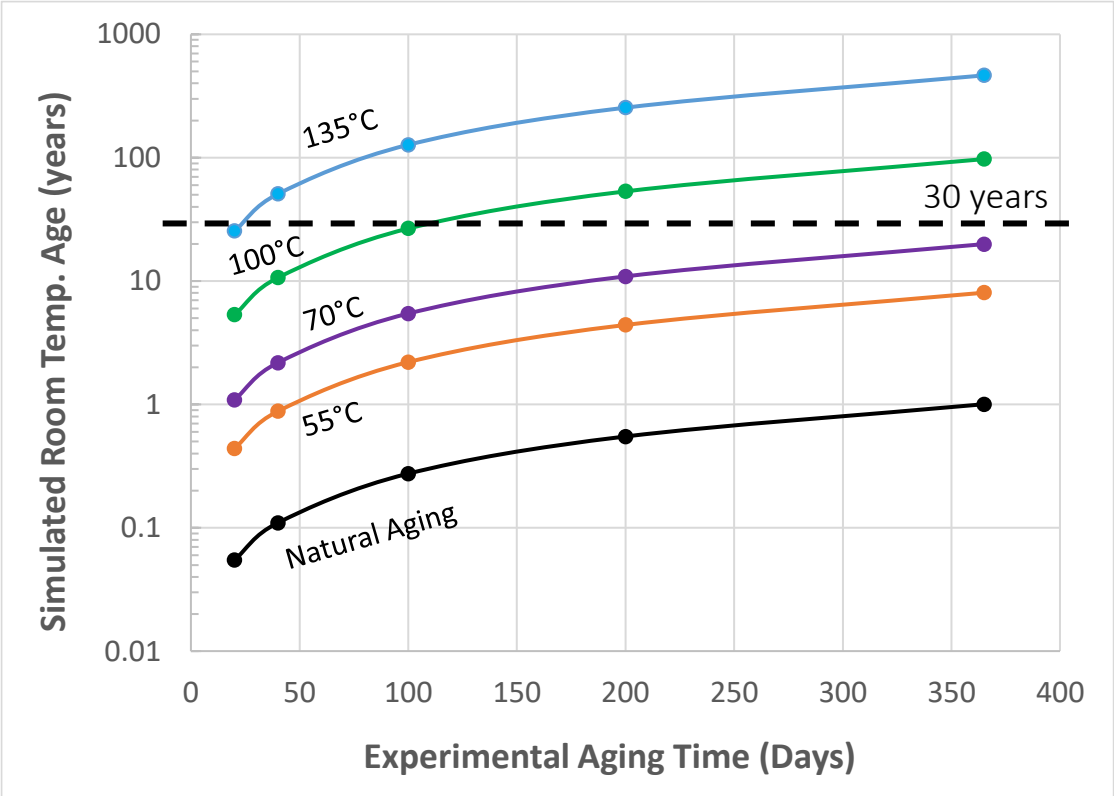

Fig. 9 Estimated correlation between aging time at elevated temperatures and the simulated room temperature aging based on Eqs. (3) and (4).

Mechanical Properties of Aged Sn-Pb-Sb Solder

The kinetics analysis of coarsening provides a methodology to correlate between accelerated aged solder joints and naturally aged 30-year-old soldered assemblies. Recall that an objective of this work was to determine if such aging can account for the lower strength observed in the 30-year-old soldered assemblies that was shown in Fig. 2. Vickers microhardness and compression stress-strain testing were performed on natural aged and accelerated aged specimens to evaluate changes in strength. Figure 10 shows microhardness

results from specimens aged at room temperature, 55, 70, 100, and 135°C for up to 365 days. Results from B.T. Lampe [9] are also shown for this same alloy for room temperature aging of up to 60 days. For short aging times after solder solidification (inset Fig. 10), a small initial increase in hardness was observed in both the present work and the Lampe study. Beyond about 3 days of aging, a continuous decrease in hardness occurs, with the exception of the 135°C aging temperature. The initial hardness increase could be due to precipitation of Sn-rich particles within the Pb-rich phase as discussed previously (see Fig. 3). Further characterization of the short-term aged specimens would be needed to confirm this hypothesis. Microhardness values for the other aging temperatures, 55-100°C, decrease immediately due to microstructural coarsening to below hardness values obtained at room temperature. The data from the other temperatures are more clearly shown on the semi-log plot in Fig. 10b, which distinctly shows an anomalous behavior at 135°C.

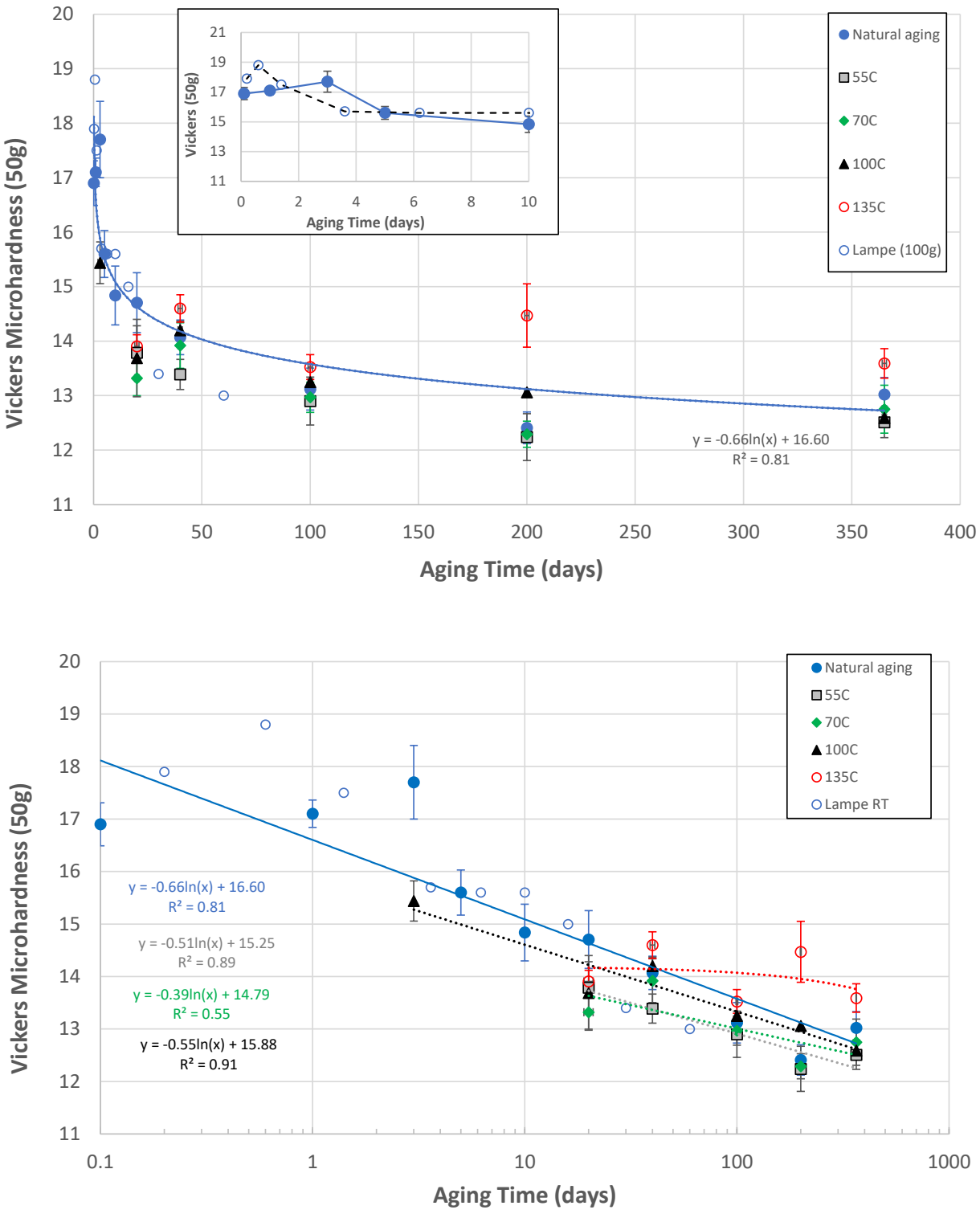

Fig. 10 a) Vickers microhardness of Sn-Pb-Sb specimens aged between Room temp. and 135°C. Inset shows hardness at early stages of aging. b) Semi-log plot of microhardness. The anomalous behavior at aging temperature of 135°C is shown, red symbols.

One approach to determine long-term aged properties is to simply extrapolate a best-fit expression of the room temperature hardness data to the 30-year natural aged condition (blue curve, Fig. 10). The assumption is made that the decrease in microhardness follows a similar trend, on a percentage basis, to that for the strength of the soldered assemblies (Figs 1-2). Extrapolation of the best-fit equation in Fig. 10 gives Vickers microhardness of ~10.5 HVN after 30 years of aging. This value can be compared to the original hardness and correlated to the aged solder assembly results in Fig. 2 but recall that a stabilization treatment of 20 days at room temperature was applied prior to testing the original soldered assemblies. Therefore, the 30-year hardness estimate should be compared to the 20-day room temperature hardness value of ~14.7 HVN. Thus, the best-fit prediction based on microhardness is 10.5/14.7 or 71.4% of the original hardness value. This prediction is somewhat low when correlated to the 30-yr. aged strength results in Fig. 2 (on average 3058 lbs. or 87% of the original mean force of 3507 lbs.) but it does fall within the lower end of the range (lowest value of 2455 lbs. or 70% of the original strength). Thus, direct extrapolation provides a reasonable, albeit conservative, prediction of mechanical properties for use in design purposes.

An alternative approach is to use the accelerated aging data and microstructural rate kinetics analysis discussed above. The microhardness results are chosen for candidate aging conditions, for example 100 days at 100°C or 365 days at 70°C (Figs. 7 and 9) and compared to the 20-day room temperature microhardness. The microhardness prediction is 12.75 - 13.25 HV or 87 - 90% of the as-soldered + stabilized condition. This prediction falls very well within the aged results for the as-soldered assemblies shown in Fig. 2. See also the summary below in Fig. 12.

A similar approach was taken with the compressive stress-strain tests. Figure 11 exhibits the compressive yield strengths (YS) in the same format as Fig. 10. The compressive YS for the accelerated aged specimens fell consistently below the room temperature aged YS, again with the exception of the 135°C results, which was similar to the microhardness behavior. Also shown in Fig. 11 are the *shear* test results from B.T. Lampe for up to 60 days of aging at room temperature. The shear strength displayed a small increase at very short aging times, whereas the compressive yield strengths in the present study did not. The remainder of the Lampe shear strength values followed a trend similar to that found for compressive YS, with the shear strength values being 0.70 - 0.85 of the room temperature compressive yield strengths. A best-fit and direct extrapolation of the room temperature compressive YS predicts 27.9 MPa (4041 psi) for 30 years of aging. This represents 66% of the as-soldered plus stabilized compressive yield strength. The alternative approach utilized the compressive YS values pertaining to 100°C for 100 days or 70°C for 365 days, as was done with the microhardness data. The compressive YS values are 32.9 - 36.4 MPa (4772 – 5279 psi) or 78 to 86% of the as-soldered plus 20-day stabilized compressive YS values.

A summary of the predictions is presented in Fig. 12 for both microhardness and compressive YS with their correlation to the actual 30-year aged mechanical test results for the soldered assemblies (Figs. 1-2). Again, the assumption is made that microstructural coarsening would lead to similar reductions in properties among the various mechanical tests, that is, microhardness and compressive testing of laboratory specimens as well as pull-testing of the fielded soldered assemblies. For both hardness and compression testing, extrapolation of the RT aging curves gives conservative (low) estimations of the 30-year aged strength of soldered

assemblies. This finding suggests a functional form in which the long-term aging behavior follows a “flatter” trend then either a logarithmic or power law equation, Figs. 10 and 11. In contrast, the comparisons based on accelerated aging tests and microstructural aging kinetics, e.g. 100 days at 100C or 365 days at 70C, give predictions well within the observed strengths of the 30-year solder assemblies. These predictions validate the assertion that microstructural coarsening, which results from solid-state aging, is correlated to the changing mechanical properties of the Sn-Pb-Sb solder, not only for the test specimens in the present study, but also for the actual 30-year aged solder assemblies.

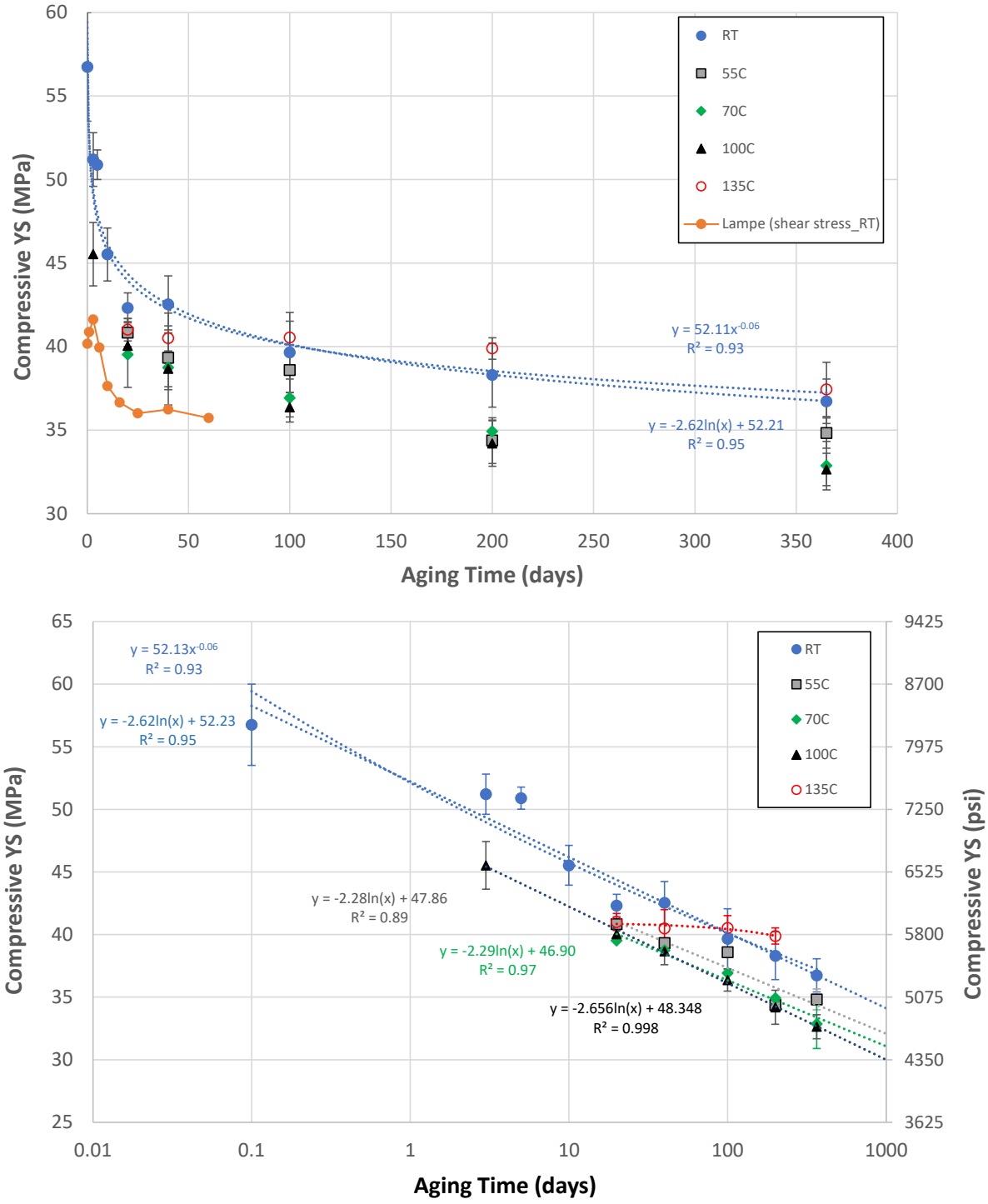

Fig. 11 a) Compressive yield strength of Sn-Pb-Sb specimens aged between Room temp. and 135°C, with B.T Lampe shear strength data for comparison [9]. b) Semi-log plot of compressive YS. Note the anomalous behavior at aging temperature of 135°C, red symbols.

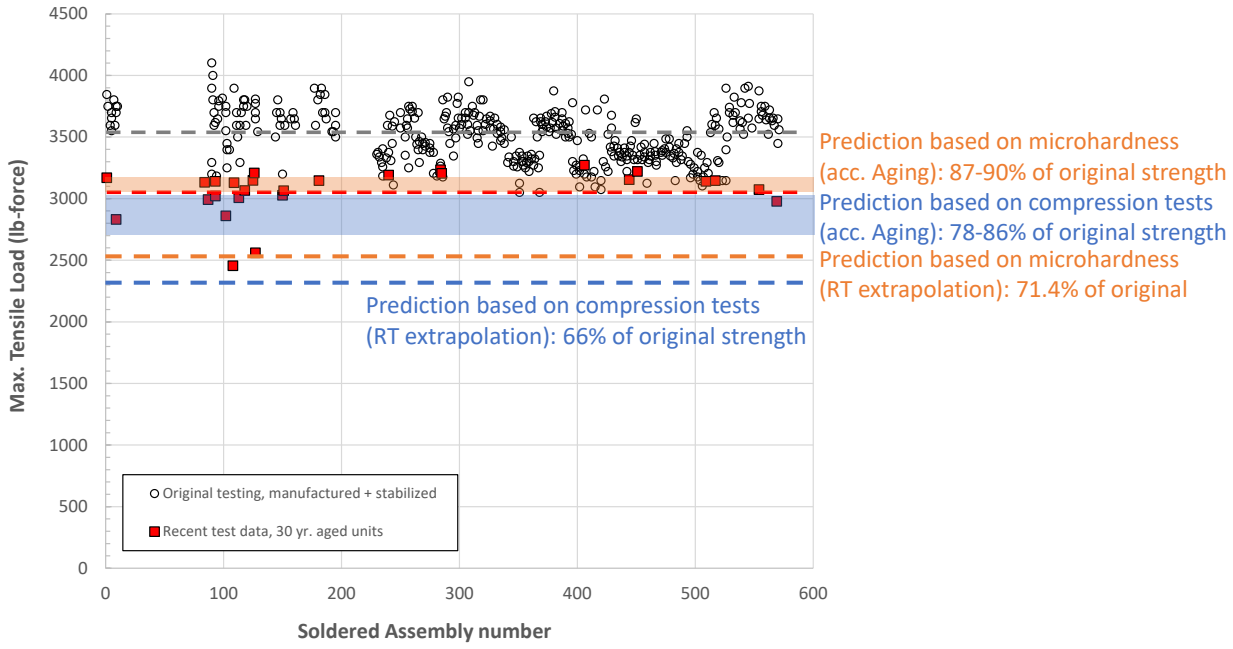

Fig. 12. Summary of predicted 30-year aged properties of Sn-Pb-Sb solder. Predictions are based on 1) Extrapolated best-fit equations of R.T. aged microhardness and compressive YS and 2) Accelerated aging microhardness and YS and correlated microstructure coarsening kinetics.

While a 13% drop in average strength after 30 years may seem minor, it is important to recall the comparison is being made to the 20-day room temperature (or 3 days at 100°C) stabilized condition, not the "as-soldered" condition. Based on Figs. 10 and 11, when the decreased strength (or hardness) is compared to the *peak strength* condition -- a few hours after soldering -- the strength losses are in the range of 29-41% after 30 years (59-71% of the peak strength). Thus, microstructural coarsening in fact generates a significant drop in strength. Perhaps the reason this is not a larger concern is that typical laboratory testing does not take place within hours or even a few days of soldering. In other words, it could be argued

that the vast majority of mechanical property data in the literature for the “as-soldered” condition in reality represents properties in a “stabilized” condition -- along the more gradual slope of the hardness or strength curves in Figs. 10 and 11. While additional minor aging effects are certainly expected, the magnitude of those changes is much less than would be otherwise observed if testing were performed immediately or very soon after solder solidification. The effect is akin to that observed in aluminum alloys subjected to natural aging (T4 condition). In that case, hardening/strengthening takes place due to precipitation at room temperature but the major strengthening occurs within the first few days or weeks [40]. Only minor additional changes in strength are expected in the long-term.

Another aspect of solder aging is discussed here. When at room temperature, the solder will continue to age indefinitely so the microstructure will change at longer aging times. For specimens accelerated aged at high temperatures, subsequent room temperature aging may take place, depending on the prior accelerated aging temperature and time duration. Aging at temperatures of 100-135°C is expected to allow very little subsequent microstructural changes at room temperature because coarsening has taken place in a majority of the Pb-rich phase. However, for lower aging temperatures such as 55°C, additional changes could potentially occur in the microstructure at room temperature. Further work would be needed to confirm the latter hypothesis as a function of accelerated aging temperature and time.

Finally, a discussion is made with regard to the 135°C aging condition. Anomalous behavior for the 135°C aging condition appeared in Figs. 10 and 11. Rather than following the trend of decreasing strength with increasing temperature, holding at 135°C generates a strength increase as a function of aging time. Higher resolution SEM imaging was performed on

specimens aged at 135°C and compared to those resulting from aging at 55°C; see Fig. 13. Fine-scale precipitation is observed within the Sn-rich matrix phase after aging at 135°C while no precipitates are found in the 55°C specimen. The 135°C precipitates appear to align in crystallographic directions, although further analysis would be required to fully characterize the precipitate arrangement as well as the composition of the precipitates. A second observation was made from the SEM images in Fig. 13. Regions of discontinuous (lamellar) precipitation/coarsening were noted along some grain boundaries within the Sn-rich phase aged at 135°C. This phenomenon represents another microstructural aging mechanism not found at lower aging temperatures.

In summary, a fine-scale precipitation mechanism observed in Fig. 13 is a plausible explanation for the long-term hardening (after initial strength losses at short times) at 135°C. The phenomena observed in Fig. 13 reiterate the need for prudence when selecting severe accelerated aging conditions because they can activate microstructural changes that are not relevant to lower aging temperatures experienced in an application.

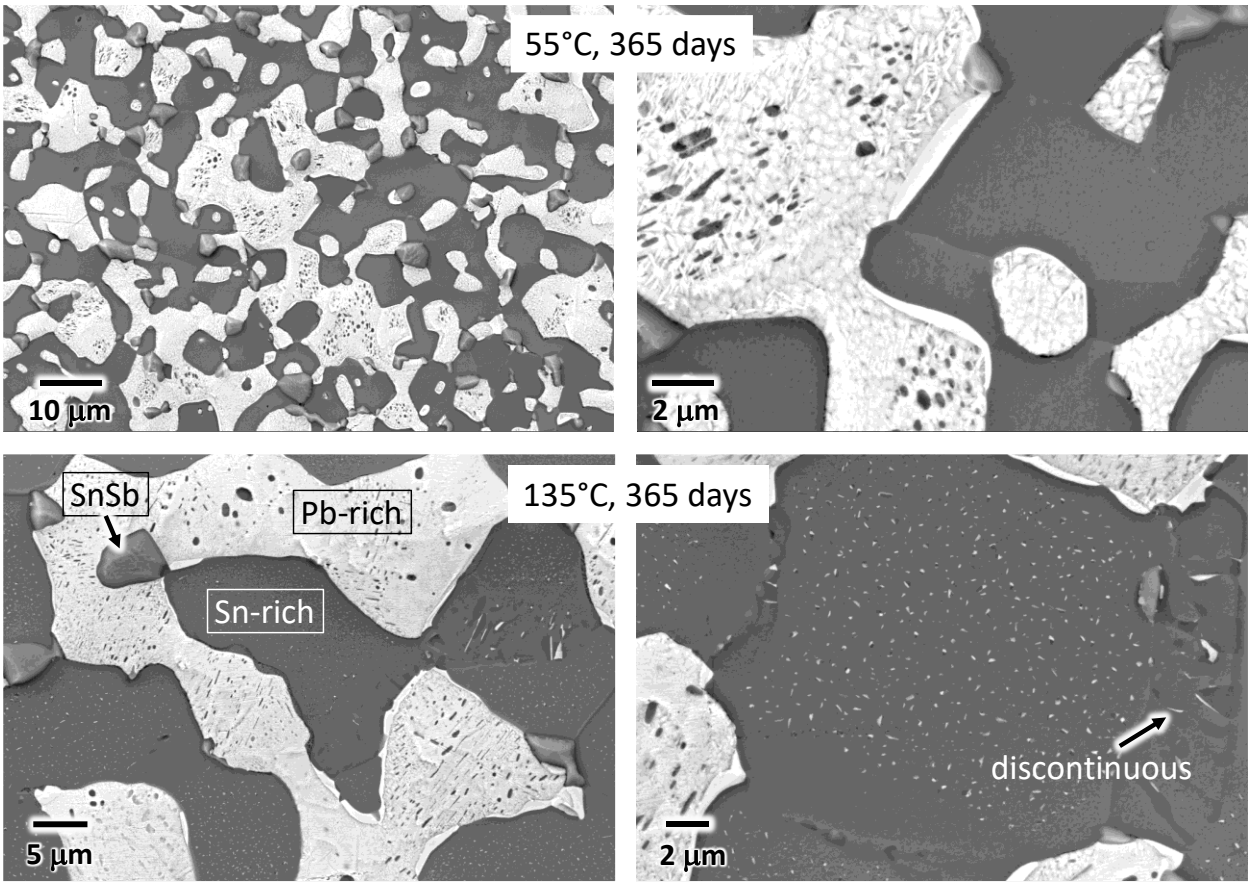

Fig. 13. SEM/BSE micrographs of 55°C and 135°C aged specimens. Fine-scale precipitation is found within the Sn-rich phase regions at 135°C aging. Regions of discontinuous precipitation are also found at some grain boundaries for 135°C aging.

Conclusions

Accelerated aging experiments were performed on 50Sn-47Pb-3Sb (wt %) solder in order to simulate the microstructure and mechanical properties observed in actual 30-year aged solder joints. A kinetic analysis was performed on the microstructural coarsening of this solder alloy. The following conclusions were drawn from these studies.

1. Solder aging experiments were performed at room temperature, 55, 70, 100, and 135°C for up to 365 days. Based on Pb-rich phase size, x, the following kinetic equation was developed for aging of 50Sn-47Pb-3Sb (wt %) solder:

$$x = 3.75 \times 10^{-6} + 8.5 \times 10^{-5}\, t^{0.43} \exp(-24200/RT)$$

2. Comparisons between accelerated aged microstructures and 30-year naturally aged solder showed reasonable agreement when correlated with the kinetic analysis. For Sn-Pb-Sb solder, the accelerated aging conditions of 100 days at 100°C can be used to simulate 30 years of natural aging.

3. Compression testing and Vickers microhardness showed significant strength loss within the first 20-30 days after soldering; then, the microstructure and mechanical properties changed more slowly over long periods of time. By combining accelerated aging data and the microstructure-based kinetics, strength predictions were made that match well with the properties of the actual soldered assemblies naturally aged for 30 years.

4. Aging at the highest temperature of 135°C produced anomalous results, with hardness and strength increasing as a function of time. This behavior was found to be due to additional precipitation reactions occurring at this temperature. Caution should be used when selecting severe accelerated aging conditions because they can activate microstructural changes that are not relevant to lower aging temperatures experienced in service.

Acknowledgements

The authors wish to thank Dr. H. Fowler and Dr. P.T. Vianco for careful review of the manuscript. Thanks to Dr. D. Balch and J. Morfa for support of this work. Sandia National Laboratories is a multimission laboratory managed and operated by National Technology and Engineering Solutions of Sandia LLC, a wholly owned subsidiary of Honeywell International Inc. for the U.S. Department of Energy's National Nuclear Security Administration under contract DE-NA0003525. The views expressed in the article do not necessarily represent the views of the U.S. Department of Energy or the United States Government.

References

1. K. Jung, H. Conrad, Microstructure Coarsening during Static Annealing of 60Sn40Pb Solder Joints: I Stereology. J. Elec. Mat. **30**(10), 1294-1302 (2001).

2. K. Jung, H. Conrad, Microstructure Coarsening during Static Annealing of 60Sn40Pb Solder Joints: II Eutectic Coarsening Kinetics. J. Elec. Mat. **30**(10), 1303-1307 (2001).

3. D. Anders, C. Hesch, K. Weinberg, Computational modeling of phase separation and coarsening in solder alloys. Int. J. Solids Struct. **49**, 1557-1572 (2012).

4. I. Dutta, P. Kumar, G. Subbarayan, Microstructural Coarsening in Sn-Ag-based Solders and Its Effects on Mechanical Properties. JOM. **61**(6), 29-38 (2009).

5. A.R. Fix, W. Nüchter, Microstructural changes of lead-free solder joints during long-term ageing, thermal cycling and vibration fatigue. Solder Surf. Mount Tech. **20**(1), 13-21 (2008).

6. S.K. Kailasam, M.E. Glicksman, S.S. Mani, V.E. Fradkov, Investigation of Microstructural Coarsening in Sn-Pb Alloys. Met. Mat. Trans. A. **30A**, 1541-1547 (1999).

7. M.A. Matin, W.P. Vellinga, M.G.D. Geers, Aspects of coarsening in eutectic Sn-Pb. Acta Mat. **52**, 3474-3482 (2004).

8. F. Wang, A. Luktuke, N. Chawla, Microstructural Coarsening and Mechanical Properties of Eutectic Sn-58Bi Solder Joint During Aging, J. Elec. Mat. **50**, 6607-6614 (2021).

9. B.T. Lampe, Room Temperature Aging Properties of Some Solder Alloys. Weld. J. 330s-340s (1976).

10. H.H. Manko, Solders and Soldering: Materials, Design, Production, and Analysis for Reliable Bonding. 4th Ed. (McGraw-Hill: New York, 2001).

11. J.P. Hilger, Hardening process in ternary lead-antimony-tin alloys for battery grids. J. Power Sources. **53**, 45-51 (1995).

12. W.J. Tomlinson, N.J. Bryan, The strength of brass/Sn-Pb-Sb solder joints containing 0 to 10%Sb. J. Mat. Sci. **21**, 103-109 (1986).

13. W.J. Tomlinson, G.A. Cooper, Fracture mechanism of brass/Sn-Pb-Sb solder joints and the effect of production variables on the joint strength. J. Mat. Sci. **21**, 1730-1734 (1986).

14. W.J. Tomlinson, P.A. Rogers, The shear strength of copper and brass soldered with Sn-40%Pb containing 0 to 10% Sb and/or 0 to 15% Zn. J. Mat. Sci. **22**, 2416-2420 (1987).

15. W. Wang, F. Dai, B. Wei, Formation mechanism of primary phases and eutectic structures within undercooled Pb-Sb-Sn ternary alloys. Sci. China-Phys. Mech. Astron. **50**, 472-490 (2007).

16. A. Rezaee-Bazzaz, R. Mahmudi, Impression creep of Sn-40Pb-2.5Sb Peritectic Solder Alloy. Mat. Sci. Tech. **21**(7), 861-866 (2005).

17. R. Mahmudi, A. Rezaee-Bazzaz, H.R. Banaie-Fard, Investigation of Stress Exponent in the Room-Temperature Creep of Sn-40Pb-2.5Sb Solder Alloy. J. Alloys Compounds. **429**, 192-197 (2007)

18. P.T. Vianco, J.A. Rejent, A methodology to establish baseline metrics for assessing the isothermally aging of Sn-Pb solder interconnects. Solder Surf. Mount Tech. **14**(2), 26-34 (2002).

19. P. Vianco, J. Rejent, G. Zender, A. Kilgo, Kinetics of Pb-rich phase particle coarsening in Sn-Pb solder under isothermal annealing -- cooling rate dependence. J. Mater. Res. **20**(6), 1563-1573 (2005).

20. P.T. Vianco, S.N. Burchett, M.K. Neilsen, J.A. Rejent, D.R. Frear, Coarsening of the Sn-Pb Solder Microstructure in Constitutive Model-based Predictions of Solder Joint Thermal Mechanical Fatigue. J. Elec. Mat. **28**(11), 1290-1298 (1999).

21. E. Machlin, An Introduction to Aspects of Thermodynamics and Kinetics Relevant to Materials Science (Giro Press: Croton-on-Hudson, NY, USA, 1999), 299-308.

22. J.I. Goldstein et al., Scanning Electron Microscopy and X-Ray Microanalysis, 2nd Ed. (Plenum Press: New York, 1992), 190-194.

23. P.G. Kotula, M.R. Keenan, J.R. Michael, Automated Analysis of SEM X-Ray Spectral Images: A Powerful New Microanalysis Tool. Microsc. Microanal. **9**, 1-17 (2003).

24. K. Osamura, Lead-Antimony-Tin Ternary, Isothermal Section. ASM Alloy Phase Diagram Database. P. Villars Ed. (ASM International: 2006).

25. P. Shewmon, Transformations in Metals. (McGraw-Hill: New York, 1969), 63-65.

26. P. Shewmon, Diffusion in Solids, 2nd Ed., (TMS: Warrendale, PA, USA, 1989), 189-199.

27. J. Christian, The Theory of Transformations in Metals and Alloys: Part I – Equilibrium and General Kinetic Theory. (Pergamon: Oxford, UK, 1975), 541-543.

28. J. Askin, Tracer Diffusion Data. (Plenum: New York, 1970).

29. H. Mehrer, A. Seeger, Analysis of the pressure dependence of self-diffusion with applications to vacancy properties in lead. Cryst. Latt. Defects. **3**, 1 (1972).

30. D. Decker, J. Weiss, H. van Fleet, Diffusion of Sn in Pb to 30 kbar. Phys. Rev. B. **16**, 2392 (1977).

31. D. Gupta, K. Vieregge, W. Gust, Interface diffusion in eutectic Pb-Sn solder. Acta Mater. **47**, 5 (1999).

32. D. Yeh, H. Huntington, Extreme fast-diffusion system: Nickel in single-crystal tin. Phys. Rev. Lett. **53**, 1469 (1984).

33. D. Frear, D. Grivas, J.W. Morris Jr., A Microstructural Study of the Thermal Fatigue Failures of 60Sn-40Pb Solder Joints. J. Elec. Mat. **17**(2), 171-180 (1988).

34. S.N. Burchett, M.K. Neilsen, D.R. Frear, J.J. Stephens, Computational Continuum Modeling of Solder Interconnects. (Design Reliability of Solders and Solder Interconnections, R.K. Mahidhara et al. Eds., TMS: Warrendale, PA, USA, 1997).

35. D.R. Frear, S.N. Burchett, M.K. Neilsen, J.J. Stephens, Microstructurally Based Finite Element Simulation on Solder Joint Behavior. Solder Surf. Mount Tech. **9**(1), 39-42 (1997).

36. P. Hacke, A.F. Sprecher, H. Conrad, Computer Simulation of Thermo-Mechanical Fatigue of Solder Joints Including Microstructure Coarsening. J. Elec. Pack. **115**, 153-159 (1993).

37. P.L. Hacke, A.F. Sprecher, H. Conrad, Microstructure Coarsening During Thermo-Mechanical Fatigue of Pb-Sn Solder Joints. J. Elec. Mat. **26**(7), 774-782 (1997).

38. P.L. Hacke, Y. Fahmy, H. Conrad, Phase Coarsening and Crack Growth rate During Thermo-Mechanical Cycling of 63Sn37Pb Solder Joints. J. Elec. Mat. **27**(8), 941-947 (1998).

39. Z. Guo, H. Conrad, Effect of Microstructure Size on Deformation Kinetics and Thermo-Mechanical Fatigue of 63Sn37Pb Solder Joints. J. Elec. Pack. **118**, 49-54 (1996).

40. J.E. Hatch (Ed.), Aluminum: Properties and Physical Metallurgy. (ASM: Materials Park, OH, USA, 1984), 138-139.